

## Coexisting attractors in compressible Rayleigh-Bénard flow

V. M. Castillo, Wm. G. Hoover, and C. G. Hoover

*Department of Applied Science, University of California at Davis-Livermore, Livermore, California 94551-7808  
and Lawrence Livermore National Laboratory, Livermore, California 94551-7808*

(Received 10 December 1996)

We demonstrate that precise solutions of the convective flow equations for a compressible conducting viscous fluid can give degenerate stationary states. That is, two or more completely different stable flows can result for fixed stationary boundary conditions. We characterize these complex flows with finite-difference, smooth-particle methods, and high-order implicit methods. The fluids treated here are viscous conducting gases, enclosed by thermal boundaries in a gravitational field—the “Rayleigh-Bénard problem.” Degenerate solutions occur in both two- and three-dimensional simulations. This coexistence of solutions is a macroscopic manifestation of the strange attractors seen in atomistic systems far from equilibrium.

[S1063-651X(97)04405-X]

PACS number(s): 47.20.Bp, 47.27.Te, 05.45.+b, 05.70.Ln

### I. INTRODUCTION

Computer experiments, both microscopic and macroscopic, are now sufficiently detailed to compete with real laboratory experiments as sources of reliable data. Computer techniques include atomistic molecular dynamics [1–3], finite-difference [3] and finite-element methods [4], particle techniques [4,5], and higher-order implicit methods [6] for solving the partial differential equations of continuum mechanics. Intercomparisons of all these approaches make it possible to study the limiting convergence of the numerical techniques as the number of degrees of freedom is increased, as well as the corresponding consistency and agreement among the various atomistic and continuum approaches [7]. An interesting aspect of this comparison, which we emphasize here, is the coexistence of independent stationary solutions of the continuum fluid equations. For solids such a thing is no surprise, for solids have no way to forget their past history. But for fluids this lack of uniqueness is a bit unsettling. This coexistence of macroscopic hydrodynamic flow solutions is reminiscent of the complex Kolmogorov-Arnold-Moser (KAM) behavior seen in the dynamics of smooth chaotic Hamiltonian systems with only a few degrees of freedom, though again, the KAM behavior seems a more appropriate model for solids than for fluids.

The simplest continuum flow problems are the prototypes which define the shear and bulk viscosities and thermal conductivity. Next in complexity is the convective instability of a compressible fluid conducting heat in a gravitational field, “Rayleigh-Bénard” instability [1–4,8,9]. See Fig. 1. Sufficiently close to equilibrium, the hot lower boundary and the cold upper one promote Fourier heat conduction without convection. At a sufficiently high Rayleigh number, 1708 for an incompressible Boussinesq fluid [9], stable convection patterns develop for the geometry shown in the figure. In the cases discussed here, these are sets of parallel cylindrical rolls. With different boundary conditions hexagonal cells can also be observed [9].

A convective instability in the quiescent fluid leads to a steady flow just above the critical Rayleigh number. Close to the motion threshold, such a closed stationary flow is argu-

ably the simplest type of nonequilibrium flow state. Such stationary flows can be characterized, for idealized situations, close to equilibrium, by linearizing the hydrodynamic equations relative to the quiescent purely conducting state [3,9]. Lorenz’s caricature of Rayleigh-Bénard flow [10] describes not only the stationary roll structure, but also the transition to chaos, which occurs under more extreme conditions. Here we describe results found in our use of the Rayleigh-Bénard problem as a test for various alternative numerical approaches to compressible flow problems.

In the course of our investigations we found that solutions of the full set of continuum equations can be degenerate over a wide range of conditions. We first discovered the coexistence of two stable stationary flows, for the same boundary conditions, by accident, watching both develop from “random” initial conditions. Thus the computational situation is not so different from the experimental one, in which roll patterns have been observed to change on a time scale of days. Of the three flows shown in Fig. 1, the two-roll flow in a box of aspect ratio 2 is very well known. The incompressible approximation to this case has been exhaustively discussed by Chandrasekhar [9] and Busse [11].

Busse went on to explore the stability of roll patterns of various wave numbers  $\alpha$ , where  $\alpha = \pi$  corresponds to the two-roll pattern. The “Busse Bubble” refers to the region of wave number-Rayleigh number space for which roll patterns are stable. This stability region is centered near  $\alpha = \pi$  but covers a range so small as to suggest that the four-roll pattern,  $\alpha = 2\pi$ , is not stable at any Rayleigh number. Puhl and co-workers [3] presented work based on a finite-difference model of the compressible hydrodynamics equations that indicated that both one- and two-roll solutions can coexist for the same system. Additionally, they used a stability model based on the linearized hydrodynamic equations to support the existence of one-, two-, and three-roll patterns for a system with an aspect ratio equal to 2. This was for a box with four rigid sides and stress-free boundaries (otherwise odd numbers of rolls would not be possible).

Unlike Busse’s incompressible flows, the present work uses a fully compressible model, a natural choice for the study of buoyancy-driven convection. The results discussed

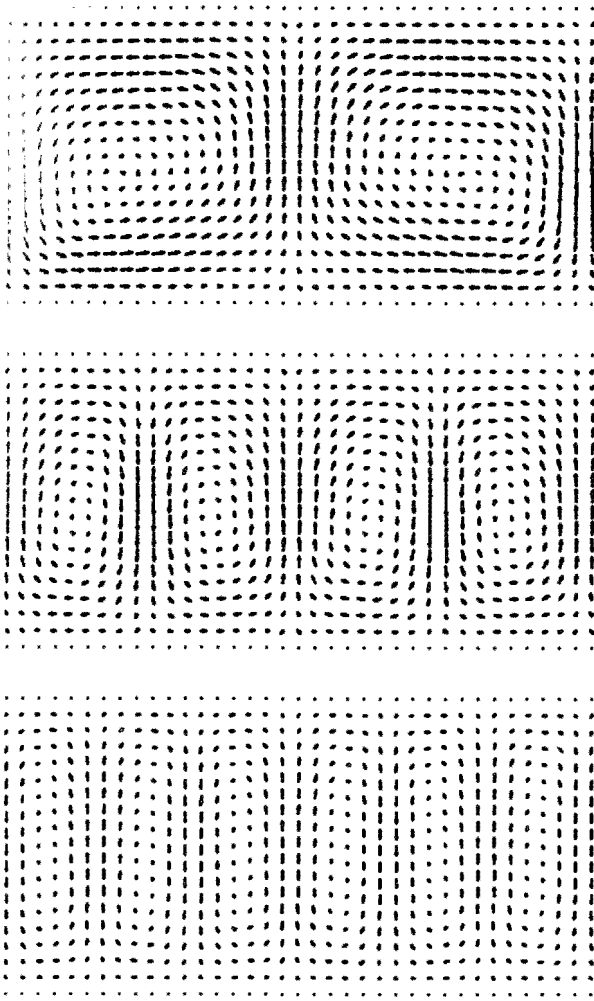


FIG. 1. Two-roll, four-roll, and six-roll stationary flows for a two-dimensional ideal gas with  $Ra=40\,000$  and Prandtl number unity. Fully stationary two-roll solutions and four-roll solutions were obtained for meshes with  $36 \times 18$ ,  $72 \times 36$ , and  $144 \times 72$  nodes. The larger meshes show also six-roll solutions.

in this paper correspond to wave numbers of  $\{\pi, 2\pi, 3\pi\}$ . In testing the robust nature of the two-roll solution, we were surprised to find that a four-roll solution would sometimes appear. Further testing showed that four-roll solutions persist, as do the two-roll ones, as the number of degrees of freedom describing the system is made arbitrarily large (at fixed Rayleigh and Prandtl numbers) for times greater than  $10^4$  sound-traversal times. In addition to showing that these patterns exist for long times, we quantitatively characterize, for all the patterns, the internal energy per unit mass, the heat flux, and the apparent linear growth rate associated with them. We extrapolated all these results to the continuum limit.

In three dimensions we found two rolls forming in a diagonal orientation, corresponding to a roll width intermediate between the two-roll and four-roll cases. There is also a fairly long-lived six-roll solution, still with exactly the same boundary conditions. See again Fig. 1. This six-roll solution is stable to a catastrophe time equal to 470 sound-traversal times, after which the system evolves to either a two- or four-roll pattern. The apparent unpredictability of the final

state suggests a complicated, fractal, boundary separating these attracting states. Additionally, persisting nonstationary, mixed-mode limit cycles have been observed to form after the catastrophe. Similar results hold in two and three dimensions, though comprehensive tests of the numerical stability in the latter case would severely strain the limits of current computers. Here we describe the methods used to obtain these solutions and present evidence that degenerate compressible solutions persist in the continuum limit. Finally, we comment on some conclusions to which this work leads.

## II. FINITE-DIFFERENCE SOLUTIONS

The continuum equations for the time development of the density, velocity, and energy per unit mass  $\{\rho, v, e\}$  can be written in terms of the "Eulerian" derivatives at fixed space locations:

$$(\partial\rho/\partial t) = -\nabla \cdot (\rho v),$$

$$(\partial v/\partial t) = -v \cdot \nabla v - (1/\rho) \nabla \cdot \sigma - g,$$

$$(\partial e/\partial t) = -v \cdot \nabla e + (1/\rho) [\nabla v : \sigma - \nabla \cdot Q].$$

It is convenient to evaluate the spatial derivatives at either the nodes or the cell centers of a regular square or cubic grid in such a way that the errors in these derivatives are second order in the grid spacing. This suggests, and our numerical results confirm, that errors in global averages will vary inversely with the number of grid points used. We investigated other higher-order methods such as a fourth-order Padé method for determining the local gradients and extrapolated values [6]. Another method investigated uses cubic splines to interpolate the state variables and determine the local gradients. This method can be shown to have errors less than the fourth power of the mesh spacing when periodic boundaries are used, but suffers a significant loss in accuracy, as do the Padé methods, near the fixed boundaries. Additionally, when the conservative form of the differential equations is used, these higher-order methods are not conservative near fixed boundaries.

All the spatial gradients which are required for the continuum equations can be expressed as centered differences of nearby nodal or cell values. The temperatures and velocities at the top and bottom boundary nodes are held fixed while the vertical boundaries are periodic. A workable scheme results [3] if nodal values of the velocity and energy and cell-centered values of density, stress tensor, and heat flux vector are used. Even with a regular Cartesian grid, there are some ambiguities in converting those terms involving both  $\sigma$  and  $\rho$  into finite-difference forms. For example, such an ambiguous term is required for a centered-difference representation of the rate at which thermodynamic work is done:

$$(\partial e/\partial t)_{\text{work}} = (1/\rho) \nabla v : \sigma.$$

In a detailed comparison of two different approaches to the two-dimensional flow equations we found that averaging the complete right-hand side at the four cell centers surrounding a node leads to somewhat smoother convergence to the continuum limit than does an alternative scheme in which  $\nabla v$  and  $(\sigma/\rho)$  are averaged separately.

At a Rayleigh number of 2500 we compared all of the eight schemes which can be generated by averaging the numerators and denominators in each of the three ambiguous terms, combined and separately. The best combination, in terms of showing the least dependence—about one-third less than the worst of the eight combinations—of the total kinetic energy on the number of grid points, used the following local averages in evaluating the time derivatives of velocity and energy:

$$\langle \nabla \cdot \sigma \rangle / \langle \rho \rangle, \quad \langle (\nabla v : \sigma) / \rho \rangle, \quad \langle (\nabla \cdot Q) / \rho \rangle.$$

The centered differences in space, averaged as just described, result in ordinary differential equations, for  $\{dv/dt, de/dt\}$  at the nodes and  $\{d\rho/dt\}$  at the cell centers. These differential equations can be conveniently and easily solved, for tens of thousands of nodes and millions of time steps, with the classic fourth-order Runge-Kutta method. The scheme conserves mass exactly.

In all of our work here, both in two and in three dimensions, we use the ideal-gas mechanical equation of state  $P = \rho kT$ , where  $k$  is Boltzmann's constant per unit mass. For simplicity, we use constant transport coefficients, with a Prandtl number of unity. By additionally choosing the gravitational field strength  $g$  consistent with constant density in the convection-free solution,  $g = k\Delta T/H$ , and with a bottom-to-top temperature difference equal to its mean, the solutions can all be characterized by the dimensionless Rayleigh number,

$$\text{Ra} \equiv gH^3 / (\nu D_T) \equiv k\Delta T(H/\nu)(H/D_T),$$

where  $g$  is the gravitational acceleration. The system height is  $H$ ; the width is  $W = 2H$ ;  $\nu$  and  $D_T$  are the kinematic viscosity and thermal diffusivity,  $\nu = \eta/\rho$  and  $D_T = \kappa/(\rho c_V)$ . We used a variety of initial conditions. If the nodal velocities are chosen randomly the corresponding kinetic energy dies out rapidly except for one or more unstable modes, which grow and lead to a finite-amplitude stationary state, of the type shown in Fig. 1. Solutions with a particular desired symmetry can be constrained to retain that symmetry in the velocity field until the other state variables converge such that fluctuations from the stationary state become numerically insignificant. Then, the constraints can be released, and the sensitivity to computational noise studied. By studying the mesh dependence of this sensitivity we found a variety of stable solutions, some of which are shown in Fig. 1.

Nodal velocities for typical solutions are plotted in Fig. 1 for a Rayleigh number of 40 000, about 23 times the critical value for two-roll convection. These solutions exhibit deviations from the fully converged continuum limit which vary smoothly with the mesh spacing, evidently as the inverse of the number of cells. Either extrapolation or the use of a relatively large number of grid points makes accurate results possible. We have based our tabulated results on series of simulations using  $2H^2$  cells, mostly with  $H = \{36, 48, 60, 72\}$ . See Table I.

For the three states shown in Fig. 1 we have estimated extrapolated continuum values for the horizontal and vertical kinetic energies, and the internal energy, per unit mass, the heat flux, and the apparent linear growth rate associated with the three types of roll patterns.

TABLE I. The horizontal and vertical contributions to the kinetic energy per unit mass, the internal energy per unit mass, the boundary heat flux, and the small-amplitude growth rate of the kinetic energy, multiplied by the system width  $W$ , are given for a series of fully converged solutions at a Rayleigh number of 40 000. Two-roll, four-roll, and six-roll solutions are compared.  $W = 2H$ .  $N = 2H^2$ . In the continuum limit energies vary as  $N$ , traversal times, diffusion times, and dissipation rates as  $N^{1/2} \propto H$ .

Rolls	$K_x/Nm$	$K_y/Nm$	$E/Nm$	$Q_{\text{boundary}}$	$W/\tau$
2	0.003730	0.00357	1.014	0.0120	1.42
4	0.001139	0.00410	1.018	0.0118	1.70
6	0.000274	0.00226	1.012	0.0106	1.25

The last two points require further discussion. In the stationary state, the horizontal average of the vertical energy flow must be constant, independent of the vertical  $y$  coordinate and equal to the rate at which heat enters (and exits) the system through the bottom (and top) boundaries. The averaged flow, including convection, but equal to the heat flux at the boundary can be computed as follows:

$$Q_{\text{boundary}} = \langle Q_y + P_{xy}v_x + P_{yy}v_y + \rho v_y [e + (v^2/2)] \rangle.$$

Numerical estimates are included in Table I.

The linear growth rate of the rolls' kinetic energy is accurately proportional to  $1/W$ , and shows relatively little additional size dependence. Rates were estimated by first determining the stationary roll-state deviations from the quiescent state. The deviations, multiplied by a small number, were then used to perturb an otherwise quiescent initial state. Growth rates could be obtained in this way with uncertainties of 1% or 2%.

Using this problem to test various numerical methods, we were able to confirm the reproducibility of the results and also reproduced some sample results given in Ref. [6]. Though the programs differed slightly for finite meshes, due to the ambiguities in differencing, as mentioned above, the independent programs agreed at the level of the results given in Table I. In appropriate special cases our two- and three-dimensional programs agreed to the full 64-bit precision used in these simulations.

### III. COMPARISON OF TWO- AND THREE-DIMENSIONAL SOLUTIONS

The extension of the two-dimensional calculations to three dimensions is relatively straightforward. We use the same mechanical equation of state as in two dimensions, and the same thermal equation of state,  $e = kT$ . The thermal diffusivity is also defined in the same way, and has the same numerical value in both cases. The viscosities require adjustment. Because, in three dimensions, a fluid without bulk viscosity is arguably the simplest, we adopt that choice in three dimensions, with the following constitutive equation:

$$\sigma_{xx} = \sigma_{eq}(\rho, e) + \eta[(4/3)\dot{\epsilon}_{xx} - (2/3)\dot{\epsilon}_{yy} - (2/3)\dot{\epsilon}_{zz}] \\ + 0[\dot{\epsilon}_{xx} + \dot{\epsilon}_{yy} + \dot{\epsilon}_{zz}], \quad \sigma_{xy} = \eta\dot{\epsilon}_{xy}.$$

The coefficients (4/3) and (2/3) do not correspond exactly to a two-dimensional ideal gas with only shear viscosity. In two dimensions a fluid with no bulk viscosity has the following constitutive relation:

$$\sigma_{xx} = \sigma_{eq}(\rho, e) + \eta[\dot{\epsilon}_{xx} - \dot{\epsilon}_{yy}] + 0[\dot{\epsilon}_{xx} + \dot{\epsilon}_{yy}], \quad \sigma_{xy} = \eta\dot{\epsilon}_{xy}.$$

The two-dimensional fluid requires an additional bulk viscosity, equal to one-third the shear viscosity, in order to correspond to the three-dimensional constitutive relation:

$$\eta_v = \eta/3 \Rightarrow \sigma_{xx} = \sigma_{eq} + \eta[(4/3)\dot{\epsilon}_{xx} - (2/3)\dot{\epsilon}_{yy}],$$

$$\sigma_{xy} = \eta\dot{\epsilon}_{xy}.$$

The numerical effect of adding the bulk viscosity in the two-dimensional simulations is typically quite small. In an ideal-gas simulation of Rayleigh-Bénard flow, at a Rayleigh number of 3600, the flow velocity increased by about one part in 1000 when the two-dimensional bulk viscosity was set equal to zero rather than to  $\eta/3$ . It is interesting, and possibly significant, that taking a two-dimensional reference system with vanishing bulk viscosity would require a negative bulk viscosity in three dimensions, leading to catastrophic instabilities.

We verified that the stationary two- and four-roll solutions from the two-dimensional work furnish stationary three-dimensional flows. This was done by using rounded-off two-dimensional solutions as initial states for three-dimensional simulations using a cubic grid. Thus the generality of our findings is not at all restricted to the two-dimensional case.

We have also investigated similar roll-type flows with smooth-particle applied mechanics (SPAM) [4,5,8]. The three-dimensional SPAM work reported here is new. The smooth-particle results are more complex, because our SPAM simulations, like molecular dynamics, fluctuate forever, and cannot reach true stationary states. In many situations the convective rolls and cells can come and go, and change orientation, in times which are quite long relative to a typical roll rotation time. A typical three-dimensional two-roll pattern, also for a Rayleigh number of 40 000, and the same constitutive model, is shown in Fig. 2. Though the stability of such two-roll patterns is well known in simulations, with both molecular dynamics [1,2] and smooth-particle applied mechanics [8], the four-roll and six-roll solutions reported in this present work remain subjects for continuing investigation in three dimensions.

#### IV. SUMMARY

The present fully converged solutions of the complete nonlinear viscous compressible conducting continuum equations establish the coexistence of several independent flow solutions, all for the same boundary conditions and the same constitutive model. Because they were discovered from randomly selected initial conditions, we know that the basins of attraction of these continuum solutions have comparable

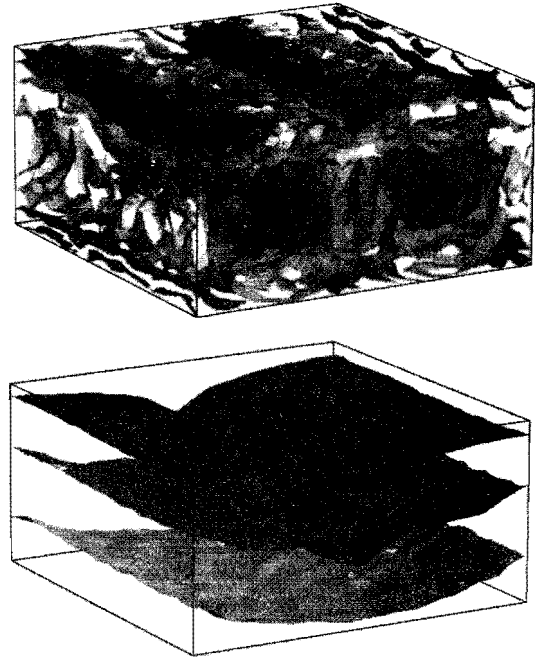


FIG. 2. Smooth-particle two-roll flow for a three-dimensional ideal gas with  $Ra=40\,000$  and Prandtl number unity. This solution uses  $36 \times 18 \times 36 = 23\,328$  smooth particles. The weighting function is Monaghan's, as described in Ref. [5], with a range equal to  $2.5(V/N)^{1/3}$ . Contours of  $(v_x^2 + v_y^2 + v_z^2)^{1/2} = \{0.03, 0.06, 0.09, 0.12\}$  and  $T = \{0.8, 1.0, 1.2\}$  are shown.

measures. No doubt the boundaries separating such basins are sufficiently complicated to frustrate any useful analysis. Unlike equilibrium thermodynamic states these nonequilibrium flows cannot be precisely compared with regard to a sensible definition of "stability" because there is no reversible path connecting them.

It is nevertheless possible to compare various aspects of the flows which have some intuitive connection with stability. Such properties include (i) the kinetic and internal energies associated with the flows; (ii) the heat fluxes, equivalent to a knowledge of the internal entropy production; (iii) the growth rates of stationary modes, as measured from infinitesimal seeds. The first two of these properties suggest the relative stability of the six-roll pattern, while the growth rate favors the four-roll pattern. The details available from computer simulations may eventually lead to correlations among these, and other, measures of relative stability. The work begun here is a modest start.

There is a logical small-scale-to-large-scale hierarchy of simulation techniques, beginning with microscopic molecular dynamics, continuing through smooth-particle applied mechanics, with its fluctuations, and concluding with fluctuation-free continuum mechanics. The instabilities which characterize macroscopic turbulence and other flows can be followed through this hierarchy. The degeneracy found here suggests strongly that the strange attractors which are pervasive in nonequilibrium time-reversible atomistic simulations [12] eventually partition large-system phase spaces into disjoint parts. Simultaneously the time reversibility and the ergodicity which characterize the smallest nonequilibrium systems are lost as the continuum limit is approached.

## ACKNOWLEDGMENTS

The advice, cooperation, and stimuli provided to us by Alan Hindmarsh, Oyeon Kum, Malek Mansour, Michel Mareschal, Harald Posch, and K. Wojciechowski were invaluable. A part of this work was performed

with the support of the Advanced Scientific Computing Initiative and the Accelerated Strategic Computing Initiative in Science and Engineering at the Lawrence Livermore National Laboratory, under the auspices of the United States Department of Energy through University of California Contract No. W-7405-Eng-48.

- 
- [1] T. Watanabe and H. Kaburaki, *Phys. Rev. E* **54**, 1504 (1996).
- [2] D. C. Rapaport, *Phys. Rev. Lett.* **60**, 2480 (1988).
- [3] A. Puhl, M. M. Mansour, and M. Mareschal, *Phys. Rev. A* **40**, 1999 (1989).
- [4] *Advances in the Free-Lagrange Method*, edited by H. E. Trease, M. J. Fitts, and W. P. Crowley, *Lecture Notes in Physics* Vol. 395 (Springer-Verlag, Berlin, 1991).
- [5] J. J. Monaghan, *Annu. Rev. Astron. Astrophys.* **30**, 543 (1992).
- [6] S. K. L  l  , *J. Comput. Phys.* **103**, 16 (1992).
- [7] Wm. G. Hoover, C. G. Hoover, O. Kum, V. M. Castillo, H. A. Posch, and S. Hess, in *Computational Methods in Science and Technology*, edited by J. Rychlewski, J. Weglarz, and K. W. Wojciechowski (Science Publishers OWN, Poznan, 1996), Vol. 2, p. 65.
- [8] O. Kum, W. G. Hoover, and H. A. Posch, *Phys. Rev. E* **52**, 4899 (1995).
- [9] S. Chandrasekhar, *Hydrodynamic and Hydromagnetic Stability* (Oxford, London, 1961).
- [10] E. N. Lorenz, *J. Atmos. Sci.* **20**, 130 (1963).
- [11] F. H. Busse, *J. Fluid Mech.* **52**, 97 (1972).
- [12] Wm. G. Hoover, *Computational Statistical Mechanics* (Elsevier, Amsterdam, 1991).